Pitting-attack behavior of cold-rolled 321 stainless steel in sodium chlorine solution at 250 °C

HAN Yun-tao[1], LV Jin-long[2], and LUO Hong-yun[3]

1. *College of Materials Science and Engineering, Beijing University of Aeronautics and Astronautics, Beijing, 100191 China (hanyuntao1985@163.com)*
2. *College of Materials Science and Engineering, Beijing University of Aeronautics and Astronautics, Beijing, 100191 China (ljlhit@126.com)*
3. *College of Materials Science and Engineering, Beijing University of Aeronautics and Astronautics, Beijing, 100191 China (luo7128@163.com)*

Abstract: Pitting-attack in steam generator tubes is one of the main degradation mechanisms that affect the life of steam generators in pressurized water reactors (PWR). In order to investigate the pitting-attack resistance of cold-rolled 321 stainless steel under severe conditions, a four-point loaded bent beam stress corrosion test in a 5 wt.**%** chloride aqueous solution (pH 8.63 at 25 **°C**), with immersing periods of 240 **hr** and 660 **hr,** at 250 **°C,** was carried out. The material microstructure was observed and analyzed with optical microscopy (OM), and the phase structure with X-ray diffraction (XRD). The morphology of the specimens after the immersing test was examined using scanning electron microscopy (SEM), and the corrosion products on the specimens' surface were analyzed through X-ray photoelectron spectroscopy. The results obtained indicated that the microstructure of the material was composed of equiaxed austenitic grains with typical annealing twins. There was an approximately 10.19 vol.**% α'**-martensite phase in the austenitic matrix. After the immersing test, specimens to which different levels of stress were applied showed different patterns of attack. When the stress applied to the specimens was below 250 **MPa**, for either 240 **hr** or 660 **hr**, only pitting-attack was detected on the surface. But when the stress was 300 **MPa** or more, pitting-attack and pitting-induced stress corrosion cracks were recognized. It was also observed that the distribution of stress on the specimens had a large influence on the pitting-attack behavior. Pitting-attacks mainly occurred around the specimens' V-notch area where the stress was concentrated. The stress distribution of the specimen was analyzed through the finite element method. The paper ends with a discussion on the mechanisms of pitting attack.

Keywords: Stress corrosion cracking; pitting attack; 321 stainless steel; Four-point loaded bent beam stress corrosion test; Sodium chloride

1. Introduction

The heat exchanger tubes that sustain the environment of the primary water at 153 **atm** and 319 **°C**, and of the steam at 282 **°C**, are one of the main components of a nuclear power plant. Throughout the power plant's operation, the tubes are partially damaged because of the severe conditions of operation. The material for the heat exchanger tube needs to have appropriate mechanical properties, especially as regards resistance to corrosion and high temperature. The heat exchanger is designed to operate for approximately 40 to 60 years. But according to previous reports[1,2], the lifetime of a nuclear power plant decreases annually because of pitting, intergranular attack, primary water stress corrosion cracking (SCC), intergranular SCC, and denting in the steam generator. In recent years, SCC and pitting-attack have occurred in boiling water reactor (BWR) and pressurized water reactor (PWR) components, such as core shrouds and primary loop recirculation (PLR) pipes fabricated with low carbon austenitic stainless steels (SS)[3-5]. Extensive analyses on these corroded components were performed and reported[3,4]. Austenitic stainless steels, which possess excellent mechanical properties and remarkable resistance to corrosion, are extensively used in various industries and line pipes for both low temperature and high temperature applications. Austenitic stainless steels, however, are very susceptible to pitting corrosion and SCC in chloride-containing solutions[6-8].

Received date: July 16, 2010
(Revised date: June 2, 2011)

Stainless steels are subject to different levels of cold work during the final manufacturing stages of components for numerous industrial applications. Cold work can affect the corrosion resistance of stainless steels because of the possible introduction of deformed substructures like planar dislocation arrays[9] and deformation twinning[10]. In addition, during the cold forming process, low nickel austenitic stainless steels can undergo a plastic, deformation-induced phase of transformation of the face-centered cubic (fcc) **γ** austenite to hexagonal closed packed (hcp) **ε** martensite and body-centered cubic (bcc) **α'** martensite. The **ε** martensite forms from randomly spaced overlapping stacking faults, and the **α'** martensite forms at shear band intersections[11]. The preferred dissolution of martensite would result in an increase in anodic dissolution and facilitate the formation of active paths for pitting initiation and growing, and for the propagation of stress-induced corrosion[12]. Peguet *et al*.[13] reported the different roles of cold work on the pitting corrosion resistance at different pitting stages, including pit initiation, propagation and repassivation. Barbucci *et al*.[14] reported that the passive currents of 304 SS in sulfate + chloride solutions significantly increased with the degree of cold work. In addition, the resistance to pitting corrosion was observed to decrease with increasing levels of cold work in a 3.5**%** sodium chloride solution[15].

In this work, we examined the microstructure of 321 SS in as-received condition, equivalent to full annealing with some cold work. We then determined the martensite phases in austenitic stainless steels and analyzed them by means of X-ray diffraction. The four-point loaded bent beam stress corrosion test was performed. The specimens endured different levels of stress, immersed in a deaerated 5 wt. **%** chloride aqueous solution for 240 **hr** and 660 **hr** in a 250 **°C** environment pressurized at 10 **MPa**. Using SEM (JSM-5800), we examined the surfaces of the specimens and we confirmed the components of corrosion products by X-ray photoelectron spectroscopy. In light of our results, we discuss the influences of different levels of stress on the initiation and spreading of pitting on the surface.

2. Experiment

2.1 Test material

The material used in this experiment was a 2 **mm** thick rectangular plate of 321 stainless steel, selected because of its widespread use across many industrial applications. The 321 SS plate was received in cold-rolled condition, equivalent to full annealing with a given degree of cold work. The chemical compositions and mechanical properties of the material, at room temperature, are detailed in Table 1, and Table 2.

Table 1 Chemical composition of the material selected (wt.%)

C	Si	Mn	P	S	Cr
0.05	0.84	1.80	0.024	0.024	17.35
Ni	Ti	Al	Mo	N	Fe
9.12	0.54	—	—	—	balance

Table 2 Mechanical properties of the material selected, at room temperature

0.2**%** Proof stress, $\sigma_{0.2}$ (**MPa**)	UTS (**MPa**)	Elongation (**%**)
300	565	55

2.2 Optical metallographic and X-ray diffraction (XRD) analyses

In order to observe the surface microstructure of 321 stainless steel, a metallographic sample was first mechanically wet-ground using a 5000 grit silicon carbide (SiC) paper, then polished with aluminum oxide (Al_2O_3) powder of 1 **μm** diameter, following which it was electrolytically etched in a 10**%** ethane diacid reagent at 12**V,** for 60 **seconds,** at 25 **°C**. After etching, the specimen was cleaned with distilled water, and afterwards dried using air. Subsequently, the specimen was examined using optical microscopy (OM). The micrographs were recorded at normal incidence.

X-ray diffraction (XRD) measurements were carried out with the Rigaku Ultima IV X-ray diffractometer. The scanning rate was 4°/**min**. We used Cu Kα (0.154056 **nm**) radiation at 40 **kV** and 40 **mA**. The experimental parameter 2θ which should be confirmed before the X-ray diffraction experiment.were measured in the range of angles from 30° to 110°.

2.3 Four-point loaded bent beam stress corrosion test

The four-point loaded bent beam stress corrosion test was performed. The bent beam specimen is used to determine the stress-induced corrosion and pitting corrosion behavior of alloy sheets and plates in different environments. The stress-corrosion test was performed following ASTM G 39 recommendations.

The geometry of a specimen used in a four-point loaded bent beam stress corrosion test is schematically shown in Fig.1. Prior to loading, the specimen was polished with 1000 grit emery paper, then ultrasonically cleaned in acetone, rinsed in deionized water, and finally dried usingair. Each specimen was then loaded to the required stress level with the specimen holder and stressing jigs. The schematic specimen holder configuration and specimen loading apparatus are shown in Fig.2. The specimen holder is made of Hastelloy alloy, selected for its excellent anti-corrosion properties. In order to prevent the galvanic action between the specimen and the holder when the stress corrosion test was conducted by immersing the specimen in electrolyte, the specimen was insulated from the holder by inserting a glass column between them. The specimen was loaded by the stressing jigs and the deflection was measured by a dial indicator, with a measuring accuracy of 0.01 **mm**. The stress for the midportion of the specimen (between contact points of the inner support) on the exterior of the four-point loaded specimens was calculated[16] using the following equation:

$$\sigma = \frac{12Ety}{(3H^2 - 4A^2)} \quad (1)$$

where **σ** is maximum tensile stress; E is modulus of elasticity; t is thickness of specimen; y is maximum deflection (between outer supports); H is distance between outer supports, and A is distance between inner and outer supports.

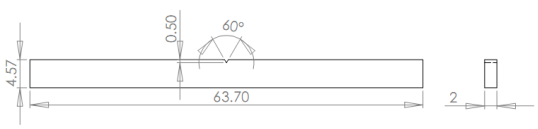

Fig.1 Geometry of a four-point loaded bent beam specimen (dimensions in **mm**).

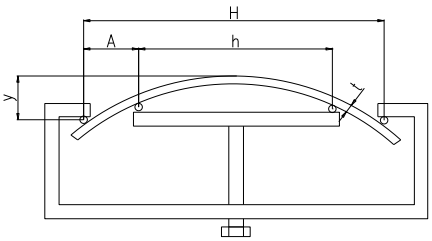

(a)

(b)

Fig.2 (a): The schematic specimen holder configuration; (b): Illustration of specimen loading apparatus.

During the immersing test, the specimens were isolated from the autoclave body. For each different testing condition, the specimens were tested in batches of three specimens per experimental run. All tests were repeated at least twice in order to ensure the repeatability and reproducibility of the results. The four-point loaded bent beam stress-corrosion test specimens were immersed in a 5 **L** Hastelloy autoclave, containing a deaerated 5 wt.**%** chloride aqueous solution (pH 8.63 at 25 **°C**), for 240 **hr** and 660 **hr,** at 250 **°C** and pressure of 10 **MPa**. The test solution was prepared with deionized water and reagent-grade sodium chloride. The test solution was adjusted to the appropriate pH by the addition of hydrogen chloride or sodium hydroxide (NaOH). The pH of the solution was determined with a JENCO 6010 pH tester. Deaeration of the test solution was achieved by purging the solution with nitrogen gas for 2**hr** prior to the test. One drawback of the four-point bent beam loading is that the specimens can only be loaded at room temperature; at high temperatures the specimens creep, resulting in a decrease in the applied load. Following recommendations in the literature[17], the specimens were loaded to a level about 10**%** higher than the actual test stress, to account for load relaxation due to elastic modules change because of heating. The applied stresses were 100 **MPa**, 150 **MPa**, 200 **MPa**, 250 **MPa**, 300 **MPa** (0.2**%** offset yield stress of metal), and 350 **MPa**. After the tests,

the specimens removed from the autoclave were examined by SEM and X-ray photoelectron spectroscopy. The corrosion products on the surface were analyzed by X-ray photoelectron spectroscopy. Afterwards, in order to examine the corroded surfaces, the corrosion products were chemically removed by washing in a 20 vol.**%** hydrogen chloride +1 vol.**%** hexamethylene tetramine, at 25**°C,** for 10 **minutes**.

3. Results and discussion

3.1 Optical metallographic analysis

It can be observed in Fig.3 that the microstructure of the 321 stainless steel used in this study was composed of equiaxed austenitic grains, with typical annealing twins. There was, however, some martensite in the austenitic matrix, which might have been introduced by cold work. It is well accepted that during the cold forming process, low nickel austenitic stainless steels can undergo a plastic deformation induced phase of transformation of the face-centered cubic (fcc) **γ** austenite to hexagonal closed packed (hcp) **ε** martensite and body-centered cubic (bcc) **α'** martensite. The preferred dissolution of martensite would result in an increase in anodic dissolution and facilitate the formation of active paths for pitting initiation and growing or for stress corrosion and cracking propagation.

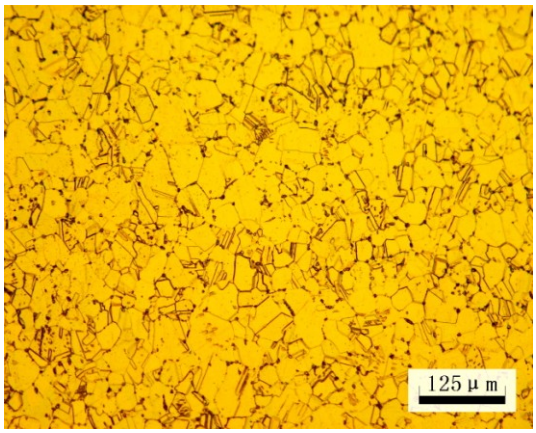

Fig.3 Microstructure of the 321 SS shows an austenitic structure and some martensite in the austenitic matrix (electrolytically etched in a 10**%** ethane diacid reagent at 12 **V** for 60 **seconds** at 25 **°C**, 200X).

3.2 X-ray diffraction (XRD) analyses

XRD analyses were used to determine the different phases and the phase content. The phase transformation was determined by the appearance of new reflections. The phase composition of a multiphase specimen was determined from the relative integrated intensities of diffraction peaks, using a direct comparison method. As suggested by Bentley and Smith[18], the integrated intensity of a diffraction line, I_i, can be expressed as:

$$I_i = KR_iV_i \tag{2}$$

Here K is a constant for a given experimental condition, independent of the diffracting substance; R_i is the constant related to the intensity factor; and V_i is the volume of the phase exposed to the X-ray beam. The volume of a certain phase V_i in a multiphase specimen can be expressed as I_i/KR_i, and the volume fraction of this phase $V_i/\sum_i V_i$, can be calculated using the following equation:

$$\frac{V_i}{\sum_{i=1}^{n} V_i} = \frac{\frac{I_i}{R_i}}{\sum_{i=1}^{n} \frac{I_i}{R_i}} \tag{3}$$

Here n is the number of phases present in the specimen.

In this study the average values of I_i/R_i from several peaks for each phase were used to calculate the phase percentage. The R_i values used in the quantitative evaluation are mainly based on the data of reference [19].

Figure 4 shows the diffractogram of the 321 SS, and the X-ray diffraction peaks information are listed in Table 3. As observed earlier, the **ε**-martensite phase is formed at the beginning of the cold-rolling and of the tension test of metastable steels. There is some evidence that the formation of **α'**-martensite is preceded by **ε**-martensite, and therefore the **γ→ε→α'** sequence is suggested. The **ε**-martensite disappears when the samples are highly deformed by rolling or by tension. The 321 SS plate selected, therefore, must have been highly pre-cold worked, and based on equation (2) and equation (3), the content of the **α'**-martensite phase in the austenitic matrix was 10.19 vol.**%**, The uncertainties in phase content given by the method mentioned above are approximately ±3 **%,** for a 95**%** confidence interval[19].

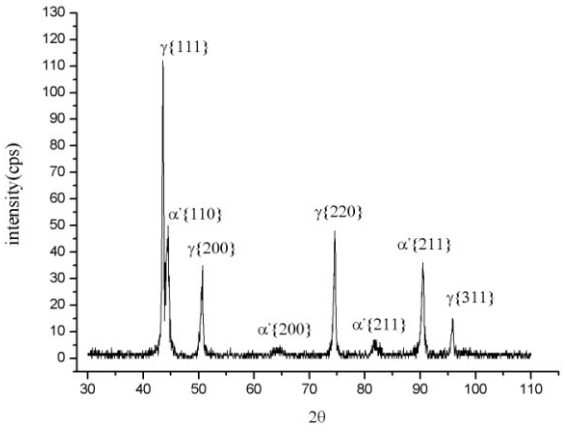

Fig.4 the X-ray diffraction pattern for the 321 SS.

Table 3 the X-ray diffraction characteristic peaks for the cold rolled 321 SS

Phase	2θ	d(Å)
{111}γ	43.596	2.0743
{110}α'	44.54	2.0326
{200}γ	50.577	1.8032
{200}α'	64.33	1.4469
{220}γ	74.616	1.2709
{211}α'	81.99	1.1742
{211}α'	90.516	1.0845
{311}γ	96.03	1.0363

Table 4 Summary of the four-point loaded bent beam stress corrosion test conditions and results (temperature: 250 °C, solution: 5 wt.%Cl⁻ aqueous solution, pH 8.63 at 25 °C, pressure of 10 MPa)

specimen number		time(**hr**)	applied stress (**MPa**)	modes of attack
test 1	test 2			
A1,A2,A3	a1,a2,a3	240	100	Pitting-attack
B1,B2,B3	b1,b2,b3	240	150	Pitting-attack
C1,C2,C3	c1,c2,c3	660	200	Pitting-attack
D1,D2,D3	d1,d2,d3	660	250	Pitting-attack
E1,E2,E3	e1,e2,e3	660	300	Pitting-attack and pitting-induced stress corrosion crack
F1,F2,F3	f1,f2,f3	660	350	Pitting-attack and pitting-induced stress corrosion crack

3.3 Four-point loaded bent beam stress corrosion test

3.3.1 Different modes of attack

In a 5 wt.**%** chloride aqueous solution, at 250 °C and pressure of 10 **MPa**, the four-point loaded bent beam specimens that were applied different levels of stress showed different modes of attack. When the stress applied on the specimens was below 250 **MPa**, whether the immersing period was 240 **hr** or 660 **hr**, only pitting-attack was detected on the surface. However, when the stress applied was of 300 **MPa** or above, both pitting-attack and pitting-induced stress corrosion cracks were observed, as shown in Table 4. Therefore the stress applied on the specimen and the immersing time were the important factors influencing the modes of attack.

For austenitic stainless steel, pitting corrosion is most prevalent in environments containing chloride. The pitting occurs aggressively on the surface of the specimen and propagates towards the direction perpendicular to the applied stress, as shown in Fig.5.

Figure 5 (a) shows the state of specimen B2, subjected to corrosion during 240h, in a 5 wt.**%** chloride aqueous solution. After the corrosion products were removed, it was obvious that pitting-attack had occurred, but no corrosion cracks from stress were observed. The diameter of the pittings was approximately 15-20 **μm**. SCC was observed in all of the specimens tested during 660**hr** at 300 **MPa** and 350 **MPa**. Figure 5 (b) shows some shallow stress corrosion cracks induced by pitting. They are mainly distributed around the pitting and close to each other. Because of the interactions of the microcracks, they may coalesce together and become a major crack. Figure 5 (c) is the photograph of SEM that shows another initiation mode of SCC induced by pitting. SCC spread from the bottom of the pitting after a 350 **MPa** stress was applied. The length of SCC was approximately 25-40 **μm**. Figure 6 shows the main elements of the corrosion products on specimen E3. They were a mixture of iron and chromium oxides.

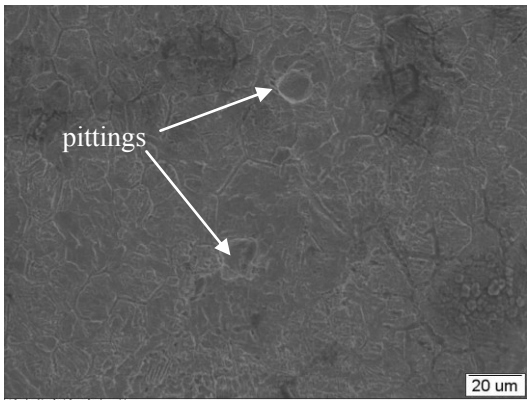

(a)

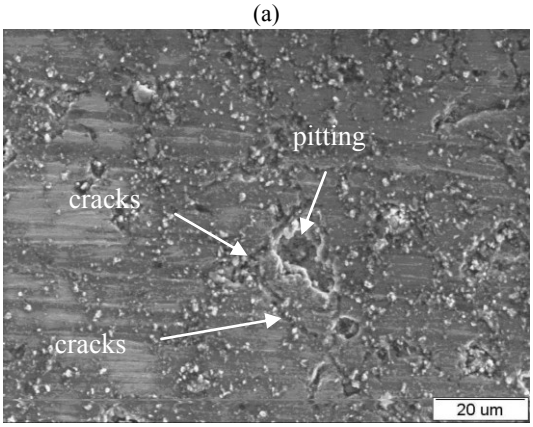

(b)

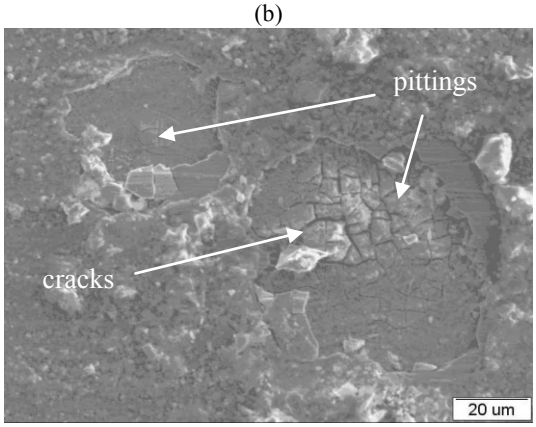

(c)

Fig.5 SEM micrographs showing the different modes of attacks in 5 wt.**%** Cl^- aqueous solution at 250 **°C** pressurized to 10 **MPa**: (a) specimen B2, (b) specimen E3, (c) specimen f1.

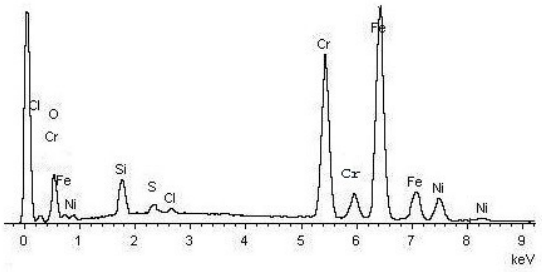

Fig.6 X-ray photoelectron spectroscopy analysis of corrosion products on specimen E3.

3.3.2 The effects of the stress distribution on the pit size and their number, in different areas of the specimen

Pitting-attacks were observed in all of the specimens tested in the 5 wt.**%** chloride aqueous solution for the experiment times of 240 **hr** or 660 **hr**, irrespectively of the level of the applied stress. Pitting corrosion is most prevalent in chloride-containing environments, and easily occurs in vulnerable areas on the surface, especially when high level tensile stress is applied.

SEM observations of the specimens that had been immersed in the autoclave for 240**hr** were performed to study the effects of the stress distribution on the specimen, the pitting size, and their number in different zones of a specimen (Fig.7). The specimens showed significant changes in the size and number of corrosion pits in different zones. Approximately 50 large pits with a diameter in the range of 10–30 **μm** were found within zone A on the specimen surface. (Fig.8 (a)). But zone B and zone C of the specimen surface were only slightly corroded, as shown in Fig.8 (b) and (c).

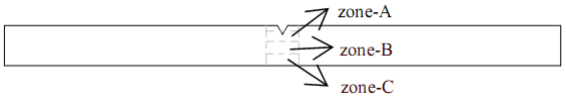

Fig.7 different zones of the specimen for SEM observation.

In order to quantify the pitting behavior, analyses of the SEM camera images were performed, using the image-processing software AxioVision R4.4 with the following procedure[20]: (1) bipolarization of the SEM camera image by brightness, (2) filtering of the bipolarized images, and (3) modeling of the pittings. Afterwards, the software could display the diameter, the area and the number of pittings. Figure 9 shows the significant changes in the number of pittings within different zones of the specimen B2. This may be attributed to the differences in the microstructures of different zones. However, the stress distribution on the specimen could be the key point. In order to investigate the stress distribution on the specimen, finite element analyses (FEA) were carried out. The size of the plate was confirmed according to the dimension of the specimen. A bent load was subjected to the plate. Elastic analyses were performed under the condition of a Poisson's ratio of 0.3, using the

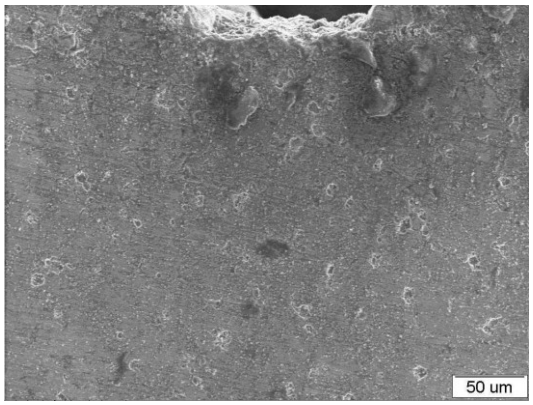

(a)

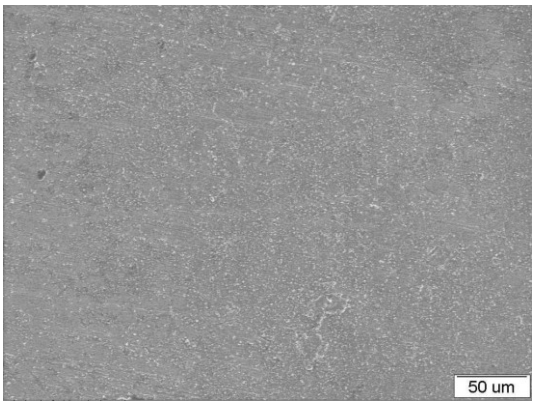

(b)

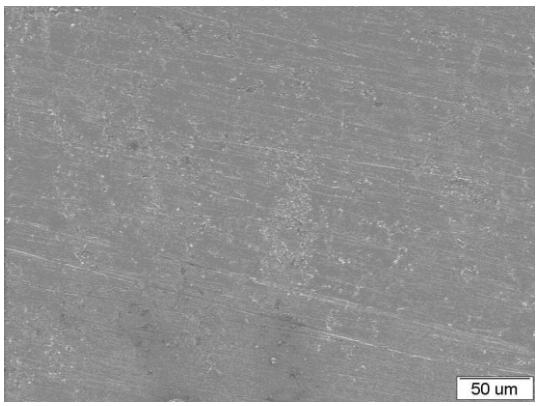

(c)

Fig.8 SEM images of the pitted surface for the specimen B2 (a) zone-A, (b) zone-B, (c) zone-C.

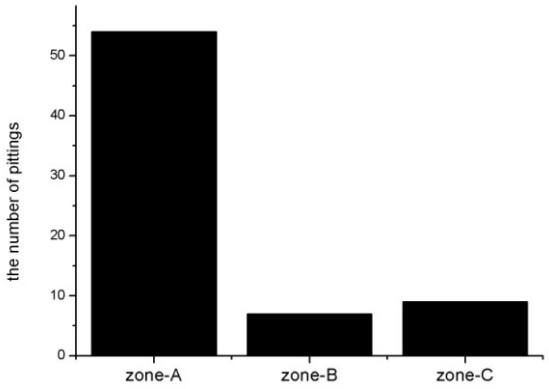

Fig.9 The number of pittings within different zones of the specimen B2

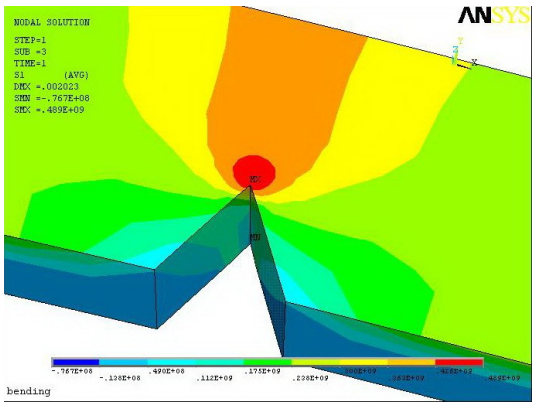

(a)

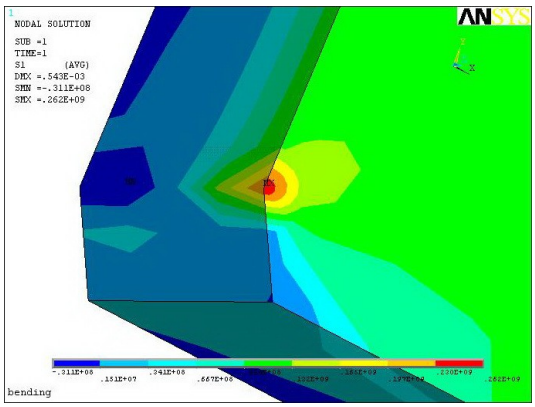

(b)

Fig.10 stress distribution on the specimen obtained by the simulation: (a) the whole specimen; (b) the V-notch tip.

general-purpose finite element program ANSYS, Version 11.0. Figure 10 shows the results of stress distribution on the specimen, obtained by simulation. The stress distribution maps exhibited relatively large stresses at V-notch tips and there was a stress relaxation zone widely distributed around the area away from the V-notch. The high stress around the V-notch tips contributed to new pitting and made the existing pittings grow bigger and deeper, as shown in Fig.8 (a). Although in the area away from the V-notch the stress was relatively small, there were a few pittings initiated. Therefore stress applied on the specimen was a vital factor in influencing the initiation and growth of the pitting.

3.4 Mechanisms of pitting-attack

Pitting is a form of localized corrosion in which metal is removed, especially from vulnerable areas on the surface. More specifically, pitting corrosion is a local dissolution leading to the formation of cavities in passivated metals or alloys that are exposed to aqueous, nearly neutral solutions containing

aggressive anions like, for example, chloride. Over the past decades, abundant work has been carried out in order to study the initiation and the growth of pitting on traditional materials.

Although there are many models of piting attack, they can be sorted into three main groups[21]. In the first group of models, it is proposed that before the pit nucleation (local dissolution of metal), penetration of chloride occurs without destroying the passive film. Dissolution of the metal occurs when the chloride reaches the metal. Another group of models postulates that mechanical breakdown of the passive film precedes the local dissolution of the metal and the developing pit. Still another group of models assume local thinning of the passive film, until the bare metal is uncovered. Furthermore, four stages of pitting corrosion can be distinguished[22]: (i) processes occurring on the passive film, at the boundary of the passive film and of the solution; (ii) processes occurring within the passive film; (iii) formation of a so-called metastable pit, which develops and grows for a short period of time below the pitting potential and then repassivates (this is an intermediate step in pitting); (iv) stable pit growth following the pitting potential.

Some researchers believe that the first step in pit initiation is mechanical breakdown of the film, and that the stress applied to the specimen is a critical factor. Hoar[23] assumed that in contact with an aggressive electrolyte, the passive film becomes mechanically stressed and damaged by pores and flaws, which are the result of changes in the interfacial forces. According to Sato[24], breakdown occurs as the film attains the thickness at which the mechanical stresses become critical as a result of the electrostriction pressure. Xu *et al*.[25] postulate that local mechanical breakdown of the passive film occurs in the concave regions of even a microscopically rough metal surface, through the concentration of electrostatic stresses. The models assuming a kind of mechanical destruction of the passive film, uncovering the bare metal surface, seem to be more probable. Suter and Alkire[26] observed microcracks in the Aluminum around the pitting, which provided initial sites for microcracks.

We need to acknowledge that the breakdown of the passive film phenomenon is complex, and that the effects of stress on the occurrence and spreading of pitting are interesting, but not yet entirely understood.

4. Conclusions

Based on the above results and discussion, the following conclusions can be drawn:

1. The microstructure of the 321 stainless steel used in this study was composed of equiaxed austenitic grains with typical annealing twins. According to the XRD analysis, about 10.19 vol.**%** **α'**-martensite phase was found in the austenitic matrix.
2. In a 5 wt.**%** chloride aqueous solution at 250 **°C**, with pressure of 10 **MPa**, the four-point loaded bent beam specimens to which different levels of stress were applied showed different modes of attack. When the stress applied to the specimens was below 250 **MPa**, whether the immersing period was 240 **hr** or 660 **hr**, pitting-attack solely was detected on the surface.
3. When the stress was of 300 **MPa** or above, both pitting-attack and pitting-induced stress corrosion cracks were recognized.
4. Based on the the FEA simulation, there was a stress concentration at V-notch tips and there was a stress relaxation zone widely distributed around the area away from the V-notch. Consequently the specimens showed significant changes in the size and number of corrosion pits in different areas. Approximately 50 large pits with a diameter in the range of 10–30 **μm** were found within zone A. Zone B and zone C of the specimen surface, however, were only slightly corroded.
5. Stress is one of the key factors influencing the initiation and growth of pitting.
6. There are three groups of models for pitting attack. The phenomenon of the breakdown of the passive film is complex, and the effects of stress on the initiation and growth of pitting are not yet clearly understood. Further research needs to be carried out in order to elucidate the remaining questions.

Acknowledgement

This study was partly supported by the Major Project of Chinese National Programs for Fundamental Research and Development (973 Program, 2006CB60500).

References

[1] DOUECKE R., ODAR S., and STELLWAY, B.: Operating Experience with Steam Generator, Service Report Power Plants, 1989.

[2] PIERSON, E., STUBBE, J., DENY, G., and LABORELEC: Stress Corrosion Cracking of Alloys 690, 800 and 600 in Acid Environments Containing Copper Oxides, CORROSION, 1996, 96, 24-29.

[3] SHOJI, T.: Progress in the Mechanistic Understanding of BWR SCC and its Implication to the Prediction of SCC Growth Behavior in Plants, in: Proc. 11th Int. Symposium. Environ. Degradation of Materials in Nuclear Power Systems-Water Reactors, ANS, 2003, 588.

[4] KUMAGAI, K., SUZUKI, S., MIZUTANI, J., SHITARA, C., YONEKURA, K., MASUDA, M., and FUTAMI, T.: Evaluation of IGSCC Growth Behavior of 316NG PLR Piping in BWR, in: Wang, Y. Y. (Ed.), Residual Stress, Fracture, and Stress Corrosion Cracking, PVP-vol.479, ASME, 2004, 217.

[5] ANGELIU, T. M., ANDRESEN, P. L., HALL, E., SUTLIF, J.A., SITZMAN, S., and HORN, R.M.: Intergranular Stress Corrosion Cracking of Unsensitized Stainless Steels in BWR Environments, in: Ford, F. P. Bruemmer, S. M., and Was, G. S. (Eds.), Proc. 9th Int. Symposium Environ. Degradation of Materials Nuclear Power Systems-Water Reactors, TMS, 1999, 311.

[6] CHEN, H., CHU, W.Y., GAO, K.W., and QIAO, L.J.: Effect of Hydrogen-induced Martensite on Stress Corrosion Cracking of Type 304 Stainless Steel in Boiling $MgCl_2$, Journal of Materials Science Letters, 2002, 21(17): 1337-1338.

[7] ALYOUSIF, O.M., and NISHIMURA, R.: The Stress Corrosion Cracking Behavior of Austenitic Stainless Steels in Boiling Magnesium Chloride Solutions. Corrosion Science, 2007, 49(7): 3040-3051.

[8] ALYOUSIF, O.M., and NISHIMURA, R.: The Effect of Test Temperature on SCC Behavior of Austenitic Stainless Steels in Boiling Saturated Magnesium Chloride Solution, Corrosion Science, 2006,48(12):4283-4293.

[9] OH, Y.J., and HONG, J.H.: Nitrogen Effect on Precipitation and Sensitization in Cold-worked Type 316L(N) Stainless Steels, Journal of Nuclear Materials, 2000, 278(2-3): 242-250.

[10] LEE, T., OH, C., KIM, S., and TAKAKI, S.: Deformation Twinning in High-nitrogen Austenitic Stainless Steel, Acta Materialia, 2007, 55(11): 3649-3662.

[11] HUMBERT, M., PETIT, B., BOLLE, G., and GEY, N.: Analysis of the γ-ε-α' Variant Selection Induced by 10% Plastic Deformation in 304 Stainless Steel at 60°C, Materials Science and Engineering: A, 2007; 454-455(25): 508-517.

[12] FANG, Z., WU, Y., ZHU, R., CAO, B., and XIAO, F.: Stress Corrosion Cracking of Austenitic Type 304 Stainless Steel in Solutions of Hydrochloric acid + Sodium chloride at ambient temperature, Corrosion, 1994, 50: 873-878.

[13] PEGUET, L., MALKI, B., and BAROUX, B.: Influence of Cold Working on the Pitting Corrosion Resistance of Stainless Steels, Corrosion Science, 2007, 49(4): 1933-1948.

[14] BARBUCCI, A., CERISOLA, G., and CABOT, P. L.: Effect of Cold-working in the Passive Behavior of 304 Stainless Steel in Sulfate Media, Journal of the Electrochemical Society, 2002, 149(12): B534-B542.

[15] FU, Y., WU, X.Q., HAN, E.H., KE, W., YANG, K., and JIANG, Z.H.: Influence of Cold Work on Pitting Corrosion Behavior of a High Nitrogen Stainless Steel, Journal of the Electrochemical Society, 2008, 155(8): C455-C463.

[16] 49 Standard Practice for Preparation and Use of Bent-Beam Stress-Corrosion Test Specimens, ASTM G 39-99, 1999, 1.

[17] RICHEY, E., MORTON, D., and SCHURMAN, M.: SCC Initiation Testing of Nickel-based Alloys Using in-situ Monitored Uniaxial Tensile Specimens. The 12th International Conference on the Environmental Degradation of Materials in Nuclear Power Systems - Water Reactors -, August 14-18, 2005, Salt Lake City, Utah.

[18] BENTLEY, A.P., and SMITH, G.C.: Phase Transformation of Austenitic Stainless Steels as a Result of Cathodic Hydrogen Charging, Metallurgical and Materials Transactions A, 1986, 17(9): 1593-1599.

[19] YANG, Q., and LUO, J.L.: Martensite Transformation and Surface Cracking of Hydrogen Charged and Outgassed Type 304 Stainless Steel, Materials Science and Engineering A, 2000, 288(1): 75-83.

[20] KAMAYA, M., and HARUNA, T.: Influence of Local Stress on Initiation Behavior of Stress Corrosion Cracking for Sensitized 304 Stainless Steel, Corrosion Science, 2007, 49(8): 3303-3324.

[21] SZKLARSKA-SMIALOWSKA, Z.: Mechanism of Pit Nucleation by Electrical Breakdown of the Passive Film, Corrosion Science, 2002, 44(5): 1143-1149.

[22] MOHAMMED A. AMIN, SAYED S. ABD EL REHIM, and ESSAM E.F. EL SHERBINI: AC and DC Studies of the Pitting Corrosion of Al in Perchlorate Solutions, Electrochemical Acta, 2006, 51(22): 4754-4764.

[23] HOAR, T.P.: The Breakdown and Repair of Oxide Films on Iron, Transactions of the Faraday Society, 1949, 45: 683-693.

[24] SATO, N.: A Theory for Breakdown of Anodic Oxide Films on Metals, Electrochemical Acta, 1971, 16(10), 1683-1692.
[25] XU, Y., WANG, M., and PICKERING, H.W.: On Electric Field Induced Breakdown of Passive Films and the Mechanism of Pitting Corrosion, Journal of the Electrochemical Society, 1993, 140(12): 3448-3457.
[26] SUTER, T., TOPIN, F., and ALKIRE, R.C.: Experimental and Theoretical Studies of Pit Initiation at Single mns Inclusions in Stainless Steels, Electrochemical Society Proceedings,1999, 97(27), 425-43